Online and Offline Stability Analysis Methods for the Power Electronic-Based Components in Design and Operational Stages

Mohamadamin Salmani, *Member, IEEE*, Navid Rahbari-Asr, *Student Member, IEEE*, Chris S. Edrington, *Senior Member, IEEE*, and Mo-Yuen Chow, *Fellow, IEEE*

***Abstract*—Power electronic-based components (PECs) are at the heart of the enabling technologies for the smart-grids. They improve the controllability of the power system and provide excellent features such as load regulation, high power factor, and transient performance. However, they can behave as negative impedance due to their capability to operate as constant power loads, and jeopardize the stability of the power systems. Therefore, stability analysis of the power electronic-based distribution systems is crucial for development of the future smart-grids. This paper provides two methods to analyze stability: real-time (online) and offline. In real-time approach, the system's small-signal stability is investigated based on $d-q$ impedance measurement and unit circle criterion and by calculating source and load impedances simultaneously and in a range of frequencies. In offline approach, the system dynamics are identified from the bode plots and then based on the eigenvalue analysis, the stability of the system under different loading conditions is analyzed. Furthermore, small-signal stability of a solid state transformer (SST) as an advanced PEC with power factor correction is investigated via the proposed methods. In addition, hardware experiment is developed though power hardware-in-the-loop experiment to assess stability of an SST in load variation and validate the real-time capability of the proposed technique.**

***Index Terms*—Eigenvalue analysis, phase and gain margins, power electronic-based components, power hardware-in-the-loop, small-signal stability analysis.**

I. Introduction

A. Role of PECs in Smart-Grid and Motivation

THE smart grid concept is changing the power grid on all the stages. This concept refers to technologies used to update electricity systems with computer-based automation and control through two-way communications structures [1]. In the future electric power distribution system that is suitable for plug-and-play of distributed renewable energy resources and distributed energy storage devices power electronic-based components (PECs) are the key technologies [2]. In other words, PECs are one of the prominent enabling technologies for the future power system concepts such as smart grids and virtual power plants [3]–[6]. PECs are the main hardware platform for distributed automation of the grid. Multiple advanced management technologies proposed for automation of the smart grid [7], [8] would be realized through PECs which can exchange information through the communications network. PECs provide infrastructure and enabling technologies for power electronics-based distribution systems (PEDS). In addition, PECs enhance the characteristics of the PEDS such as power quality, voltage regulation, and power factor; however, there are some concerns with the large integration of the PECs into the distribution grids. One of the most significant concerns is the capability of these devices to operate as negative impedances while they provide constant power loads (CPLs). Generally, any electric load with the regulated output power (e.g., connected through PECs such as converters to grid) can be modeled as a CPL in the power systems. CPLs are prone to exhibit negative impedances and thus jeopardize small-signal stability of the systems. Intuitively from small-signal standpoint, negative impedance in the system has a destabilizing effect [9].

Stability analysis of the PEDS in the literature divides into three different categories: 1) steady-state, 2) small-signal, and 3) large-signal. Essentially, steady-state stability analysis is the traditional approach to the stability of the power systems and can be investigated through the equal area criterion [10]. Steady-state stability condition may be interpreted as the balance between the generated and consumed power in the system. It is worth to mention that this type of stability analysis is a prerequisite to further stability analysis. Small-signal stability is the capability of the system to return to the identical stable operating point after small disturbance occurs in the system (i.e., changes in the state variables of the PEDS). Conversely, large-signal stability (or large-scale displacement) of the system is interpreted as the ability of the system to return to any stable operating point after large displacement in the system's operating condition such as changes in the topology of the PEDS [11]. Large-signal stability of the power systems have been investigated by direct methods (i.e., Lyapunov-based techniques) or nonlinear differential equations solutions. Lyapunov techniques have been utilized for design purposes in large-scale stability assessment of specific types of PECs in [9] and [12] as well as small-signal in [13]. Since these methods addressed particular devices, they are not generic methods to be utilized for stability study of the PEDS.

Manuscript received March 6, 2015; revised May 18, 2015; accepted June 19, 2015. Date of publication June 30, 2015; date of current version November 30, 2015. This work was supported by the ERC Program of the National Science Foundation (FREEDM Systems) under Award EEC-0812121. Recommended for publication by Associate Editor Y.-M. Chen.

M. Salmani and C. S. Edrington are with the Department of Electrical Engineering, Center for Advanced Power Systems, Florida State University, Tallahassee, FL 32310 USA (e-mail: amin.salmani@gmail.com; csedrington@gmail.com).

N. Rahbari-Asr and M.-Y. Chow are with the Department of Electrical Engineering, NC State University, Raleigh, NC 27695 USA (e-mail: nrahbar@ncsu.edu; chow@ncsu.edu).

Color versions of one or more of the figures in this paper are available online at http://ieeexplore.ieee.org.

Digital Object Identifier 10.1109/TPEL.2015.2451533

In this paper, the primary goal is to ensure the stability of the PEDS from small-signal viewpoint.

B. Contributions

This paper provides two different methods for stability analysis of the PEDS. Both approaches use impedance measurement technique in the $d-q$ framework. The first method is real-time (online) method which measures the source impedance and load admittance of the PECs in real-time, and the small-signal stability of the system is investigated by generalized Nyquist criterion (GNC). This approach improves the previously developed techniques [14]–[20] by two significant features:

1) *Real-Time Capability*: It enables small-signal stability assessment of the PECs in real-time. Although real-time small-signal stability assessment of the PEDS plays a significant role in the study and control of the systems, it has not entirely been addressed and implemented to date. This method enables real time stability assessment of the PEDS by concurrent perturbations in the source and load sides of the system under test and also utilizing chirp signal for perturbation in a range of frequencies.
2) *Hardware Development*: Its simplicity to develop a powerful algorithm in hardware and software and ease of hardware implementation. The method is developed and by power hardware-in-the-loop (PHIL) experiment, the results from this experiment are verified with the simulation results. In addition, further practical considerations are discussed and added to this method, in compare to [20], in order to enable real-time capability of the method for hardware development.

The primary contribution of this study is the real-time stability analysis capability; more specifically, the ability of the proposed criterion and technique to be implemented in a real-time platform. The parallel perturbation of source and load is one of the key features of the proposed method that enables real-time capability. In addition, the proposed stability criterion, based on impedance measurement and Nyquist stability criterion, contributes higher accuracy in small-signal stability assessments of the systems by providing a complete Nyquist contour of the system's return-ration matrix. Ultimately, this yields lighter computational loads, faster computation times, and more accurate evaluation of the system's stability in a way that enables the assessment of the relative and absolute stability of the PEDS. Another advantage of the proposed technique is that it takes part of the system's nonlinearities into account by perturbing the systems with chirp signal and in a range of frequencies, instead of exclusively fundamental frequency.

The second method is offline and is based on the eigenvalue analysis of the system. For a given PEC, first the system is excited using the impedance measurement technique. Then, bode plots of the impedance matrices are drawn and the PEC dynamics in small-signal is identified. Based on the identified dynamics, an eigenvalue analysis is performed and stability criteria for the system are derived. The stability criteria are then used to assess the stability of the system under different loading conditions. Further, the stability region for the load is obtained. This approach is useful in the design stage of PECs to find their operational limits.

To validate the effectiveness of the proposed approaches, they are implemented for stability assessment of a specific PEC, solid state transformer (SST). These devices are the building blocks of the future renewable electric energy delivery and management (FREEDM) system, which is a US National Science Foundation (NSF) generation-II Engineering Research Center (ERC). FREEDM system center is a realization of a future smart-grid [2]. In addition, hardware development and experimental implementation is presented in this study. In the experimental implementation section of the proposed study, an impedance measurement unit (IMU) is developed via PHIL experiment and measures source and load impedances in real-time. Subsequently, the proposed stability criterion is implemented on the real-time digital simulator (RTDS) and by utilizing information from the developed IMU, small-signal stability of the test bed is investigated in real-time.

C. Paper Outline

This paper is organized as follows. General requirements for enhanced understanding of the small-signal stability assessment topic are presented in Section II. This is followed by stating proposed small-signal stability assessment method for real-time applications along with its practical considerations in Section III. Section IV is allocated to offline stability analysis method. Validation of the proposed stability techniques in simulation and with study of test cases for a sample system and comparison of the results are discussed in Section V. Hardware development for real-time approach is described in Section VI and experimental results are illustrated and discussed in this section. Finally, conclusion and possible future works are set forth in Section VII.

II. Preliminaries

A. Negative Impedance Characteristics of the Constant Power Loads

The improvement of power electronics technology leads to an increase in PEC penetration into the power generation, transmission, and distribution fields. These components introduce the opportunity to apply closed-loop control, which can significantly improve power, the quality of the delivered power, and also the control of the power flow, in the PEDS as well as its consequences. Generally, PECs are nonlinear devices and subsequently their dynamics are coupled with the source(s)/load(s) connected to them. In order to have a regulated output in systems highly penetrated with the PECs, control strategies and controllers have to be applied to the systems, which in turn introduce new phenomenon known as negative impedance and change the nature of stability study of the power systems [21].

Essentially, power electronics-based converters with the regulated output voltage connected to CPLs provide negative impedance characteristics at their input, since they consume constant power and work at a fixed current. Fig. 1 shows the linear approximation of the (i–v) characteristics for a CPL. Negative slope of this curve represents negative impedance.

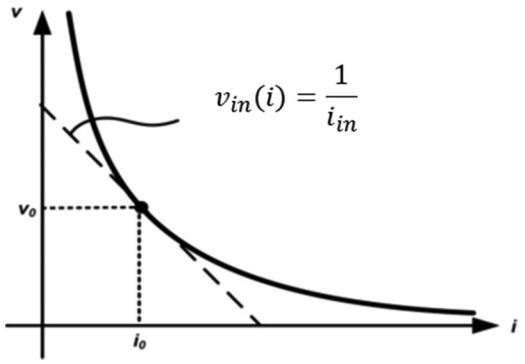

Fig. 1. Linear approximation represents negative impedance for a CPL.

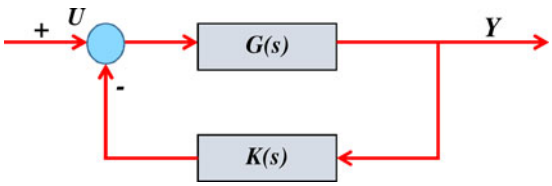

Fig. 2. General feedback system's model.

Negative impedance characteristic of the CPLs may jeopardize the small-signal stability of the PECs and in some cases the stability of the entire grid or PEDS. Generally large PEDS with higher stability inertia can be reluctant to become unstable due to instability of their components (PECs). However, it becomes a critical issue for smaller power systems such as electric ship systems, hybrid-electric vehicles, and small islanded PEDS. In these cases, the stability needs to be addressed delicately.

B. Generalized Nyquist Criterion

As it was mentioned in the prior section, increasing in integration of the PECs in distribution systems can jeopardize the small-signal stability of the PEDS. Therefore, small-signal stability investigation of the PEDS is essential. GNC is a well-developed metric to address the stability of any system (i.e., power system or PEDS) in different loading conditions [22]. This method is based on Nyquist evaluation, thus it is restated herein.

Considering the general feedback system shown in Fig. 2 transfer function (TF) of this system may be expressed by

$$H(s) = [1 + G(s).K(s)]^{-1}.G(s). \tag{1}$$

This configuration will be closed-loop stable IFF the number of right-half plane (RHP) zeroes of the $G(s)$ and $K(s)$ is equal to the counter-clockwise encirclements around point $(-1 + 0\text{j})$ of the Nyquist contour of the open-loop transfer function or $L(s)$ where $L(s) = G(s).K(s)$. $L(s)$ is also called return-ratio and $\lambda_t(s)$ represents its eigenvalues.

Considering (1), the characteristic loci of return-ratio could be defined as the graphs of the eigenvalues of the $L(s)$ (or $\lambda_t(s)$). Consequently, $1 + \lambda_t(s)$ is the eigenvalue of the $1 + L(s)$. Therefore, for the every encirclement of the point $(-1 + \text{j}0)$ by the Nyquist contour, we will have an eigenvalue on the RHP which denotes the instability of the system. The duality of the eigenvalue theorem and generalized Nyquist theorem is well-proven in [22].

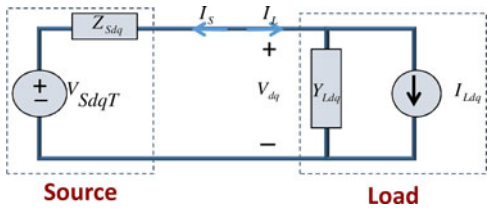

Fig. 3. Interconnected source-load power system.

After restating the Nyquist theorem, it is time to expand this theory to the power systems applications. Generally, it is possible to model every power system from source-side with their equivalent Thevenin model and from load-side with their equivalent Norton model. The interconnected source-load representation of a sample power system in synchronous $d - q$ frame is shown in Fig. 3.

This frame is utilized to facilitate computation by converting all ac variables to constant values and thus provides a quiescent operating point for linearization. The output voltage $V_{dq}(s)$ is hence determined by

$$\boldsymbol{V_{dq}}(s) = (1 + \boldsymbol{z_{Sdq}}(s).\boldsymbol{Y_{Sdq}}(s))^{-1}\boldsymbol{V_{SdqT}}(s) \tag{2}$$

where $Z_{\boldsymbol{Sdq}}$ and $Y_{\boldsymbol{Sdq}}$ are the system's source impedance and load admittance in $d - q$ frame and $\boldsymbol{V_{SdqT}}$ is the input voltage at source. Furthermore, $\boldsymbol{Z_{Sdq}}.\boldsymbol{Y_{Sdq}}$ is the return-ratio for the interconnected source-load system. This equation corresponds to the closed-loop TF of Fig. 3. Based on GNC, the interconnected source-load power system is stable, if $1 + \boldsymbol{Z_{Sdq}}(s).\boldsymbol{Y_{Sdq}}(s)$ does not have any zeros in the closed RHP. Thus, by analogy and utilizing GNC, the system is stable provided that the Nyquist evaluation of $\boldsymbol{Z_{Sdq}}.\boldsymbol{Y_{Sdq}}$ does not encircle $(-1 + \text{j}0)$ in the s-plane [19], [23].

C. Small-Signal Impedance Measurement Technique

In previous section, it was discussed that the source and load impedances are required in order to assess the stability of the power systems from small-signal viewpoint. At this part, one of the most significant methods for acquiring the source/load impedances of the PECs through the system's information (i.e., voltages and currents) is described. This technique has been developed on both ac and dc interfaces of PECs and PEDS in previous research and was widely utilized for stability studies of ac and dc systems. Generally, in a dc stability study, stability of the hybrid ac/dc system will be investigated in the dc interface; whereas in an ac stability study of the same system, the stability criterion will be analyzed from the ac interface. Furthermore, this technique is developed based on perturb-and-observe algorithm, that is to say the system is perturbed with external sources and the system's response to the perturbations are measured (observed) and based on the acquired information from the system and perturbations, it is possible to calculate the

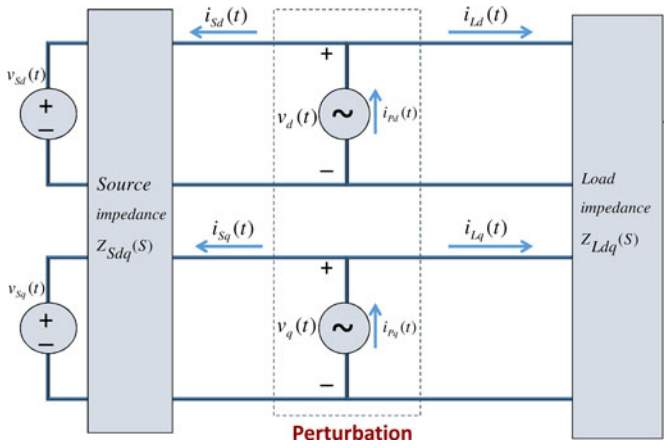

Fig. 4. Ac impedance measurement technique in the $\boldsymbol{d}-\boldsymbol{q}$ reference frame.

source and load impedance/admittance. For the ac systems, it is desirable to work in $d-q$ reference frame for two reasons: 1) work with the constant values as opposed to sinusoidal values and, 2) work with two values (since zero components are zero) instead of three values for the balanced three-phase systems. The basic algorithms for ac and dc systems are similar. The only distinction is that for ac systems two independent perturbations (i_{pq} i_{pq} i_{pd} i_{pq} and i_{pd}) are required; whereas in dc systems single perturbation is sufficient [24], [25]. Fig. 4 depicts an ac system which is considered in the $d-q$ reference frame.

In the first perturbation i_{pq} injects the current and stimulates the system while i_{pd} is set to zero. The responses are measured in the source and load sides and utilized to calculate

$$\begin{bmatrix}\tilde{v}_{d1}(s)\\ \tilde{v}_{q1}(s)\end{bmatrix} = \boldsymbol{Z_{Sdq}}(s)\begin{bmatrix}\tilde{i}_{Sd1}(s)\\ \tilde{i}_{Sq1}(s)\end{bmatrix}$$
$$\begin{bmatrix}\tilde{v}_{d1}(s)\\ \tilde{v}_{q1}(s)\end{bmatrix} = \boldsymbol{Z_{Ldq}}(s)\begin{bmatrix}\tilde{i}_{Ld1}(s)\\ \tilde{i}_{Lq1}(s)\end{bmatrix}. \quad (3)$$

In (3) $\tilde{i}_{Sd1}$ and $\tilde{i}_{Sq1}(s)$ are the system's current responses in the source interface to the first perturbation and in the d and q axes, respectively; whereas $\tilde{i}_{Ld1}$ and $\tilde{i}_{Lq1}(s)$ are the system's current responses in the load interface to the first perturbation. In addition, $\tilde{v}_{d1}(s)$ and $\tilde{v}_{q1}(s)$ are the system's voltages according to the first perturbation in the $d-q$ reference frame.

The second perturbation is made by setting i_{pq} to zero and injecting i_{pd} current. For a second time the responses in the source and load interfaces are captured/measured to acquire following equation:

$$\begin{bmatrix}\tilde{v}_{d2}(s)\\ \tilde{v}_{q2}(s)\end{bmatrix} = \boldsymbol{Z_{Sdq}}(s)\begin{bmatrix}\tilde{i}_{Sd2}(s)\\ \tilde{i}_{Sq2}(s)\end{bmatrix}$$
$$\begin{bmatrix}\tilde{v}_{d2}(s)\\ \tilde{v}_{q2}(s)\end{bmatrix} = \boldsymbol{Z_{Ldq}}(s)\begin{bmatrix}\tilde{i}_{Ld2}(s)\\ \tilde{i}_{Lq2}(s)\end{bmatrix}. \quad (4)$$

By combining (3) and (4), it is possible to find source/load impedances by

$$\boldsymbol{Z_{Sdq}}(s) = \begin{bmatrix}\tilde{v}_{d1}(s) & \tilde{v}_{d2}(s)\\ \tilde{v}_{q1}(s) & \tilde{v}_{q2}(s)\end{bmatrix}\begin{bmatrix}\tilde{i}_{Sd1}(s) & \tilde{i}_{Sd2}(s)\\ \tilde{i}_{Sq1}(s) & \tilde{i}_{Sq2}(s)\end{bmatrix}^{-1}$$
$$\boldsymbol{Z_{Ldq}}(s) = \begin{bmatrix}\tilde{v}_{d1}(s) & \tilde{v}_{d2}(s)\\ \tilde{v}_{q1}(s) & \tilde{v}_{q2}(s)\end{bmatrix}\begin{bmatrix}\tilde{i}_{Ld1}(s) & \tilde{i}_{Ld2}(s)\\ \tilde{i}_{Lq1}(s) & \tilde{i}_{Lq2}(s)\end{bmatrix}^{-1}. \quad (5)$$

By having the load impedance, the load admittance would be

$$\boldsymbol{Z_{Ldq}}(s) = \left(\boldsymbol{Y_{Ldq}}(s)\right)^{-1}. \quad (6)$$

In this technique, the system is perturbed by series voltage injection and/or shunt current injection and the system's response is measured in the source and load interfaces. Subsequently, by utilizing (3)–(6) it is possible to calculate source/load impedances in $d-q$ coordinates.

III. Real-Time/Online Stability Analysis Technique

The small-signal stability technique proposed in this section is capable to assess the stability of the PECs in real-time. This method is developed based on impedance measurement technique in $d-q$ reference frame and GNC (described in Section II). In addition, some practical considerations as well as some legitimate modification are considered to enable real-time capability of the proposed method.

A. Proposed Real-Time Stability Criterion

In this part, a novel stability assessment technique for the PECs is proposed. The proposed technique essentially investigates the small-signal stability of the PECs while they are operating. This technique is based on $d-q$ impedance measurement theory in ac interface of the PECs, and utilizes GNC to assess the stability of the systems; however, the perturbations are in a range of frequencies instead of solely system's fundamental frequency. By using generalized impedance and admittance concepts (perturbing the system in a range of frequencies), it is possible to utilize Nyquist immittance criterion for local and also regional operating points of the system; whereas the impedance matrix $\boldsymbol{Z_{Sdq}}(s)$ (or admittance matrix $\boldsymbol{Y_{Ldq}}(s)$) is a unique complex 2 by 2 matrix at any given frequency. Herein, since it is desirable to monitor a system's stability while it is operating and at any given time, the system has to be perturbed persistently and by utilizing the system's response to the perturbations, $\boldsymbol{Z_{Sdq}}(s)$ and $\boldsymbol{Y_{Ldq}}(s)$ could be calculated in a time-domain. Afterward, it is possible to transfer time-domain results to the frequency-domain by FFTs, or optionally discrete Fourier transform (DFT), and monitor the system's stability by employing the developed real-time stability criterion and technique. One of the significant privileges for the proposed method is its capability to define relative stability of the systems and compare it with the instability borders to define absolute and relative stability status of the systems.

As aforementioned, constant power nature of the PECs with regulated output voltage might cause the instability of the PEDS due to the negative impedance at the terminals [4], [5], [20]. The

proposed method investigates small-signal stability of the PECs through their ac interfaces. As it was well-described in Section II, in order to measure generalized source/load impedances of a system in ac interface, the system should be perturbed in range of frequencies and the system's response should be transferred to the $d-q$ reference frame. Generally, $d-q$ representation of the system facilitates stability analysis of the PECs through ac interfaces.

In order to explain the concept and subsequently the mathematics of the proposed method, GNC is restated herein. Considering general feedback system (see Fig. 2), where $G(s)$ and $K(s)$ are a pair of multivariable systems and their linear behavior could be represented by the state-space equation

$$\begin{aligned} \frac{dX}{dt} &= Ax + Bu \\ y &= Cx + Du. \end{aligned} \tag{7}$$

Subsequently, corresponding transfer function matrix T with inputs u and outputs y could be described as

$$T = C[sI - A]^{-1}B + D. \tag{8}$$

Fig. 3 depicts a simplified model of a PEC with ac source/load through its ac interface and in $d-q$ reference frame. It is relatively straightforward to determine the terminal voltage $V_{dq}(s)$ by utilizing basic circuit analysis techniques

$$\boldsymbol{V_{dq}}(\boldsymbol{s}) = \boldsymbol{Z_{Ldq}}(\boldsymbol{s})\left[\boldsymbol{Z_{Sdq}}(\boldsymbol{s}) + \boldsymbol{Z_{Ldq}}(\boldsymbol{s})\right]^{-1}\boldsymbol{V_{Sdq}}(\boldsymbol{s}). \tag{9}$$

This equation represents the transfer function from source voltage to terminal voltage and can be simplified as

$$\boldsymbol{V_{dq}}(\boldsymbol{s}) = \left[\boldsymbol{I} + \boldsymbol{Z_{Sdq}}(\boldsymbol{s}).\boldsymbol{Y_{Ldq}}(\boldsymbol{s})\right]^{-1}\boldsymbol{V_{Sdq}}(\boldsymbol{s}). \tag{10}$$

Back to the general feedback system, closed-loop transfer function of the system's output shown in Fig. 2 may be expressed by (1). As it was discussed hereinbefore, the small-signal stability of the closed-loop system may be determined by directly studying the return-ratio matrix defined by $L(s) = G(s).K(s)$. Therefore, the voltage stability of the $d-q$ frame model of a PEC with ac source/load, (12), may be determined by studying its return-ratio matrix

$$\boldsymbol{L_{dq}}(\boldsymbol{s}) = \boldsymbol{Z_{Sdq}}(\boldsymbol{s}).\boldsymbol{Y_{Ldq}}(\boldsymbol{s}). \tag{11}$$

Based on GNC, the transfer function represented by (11) is closed-loop stable IFF the net sum of counter-clockwise encirclements around point $(-1+0\text{j})$ by the set of characteristic loci of $L(s) = G(s).K(s)$ is equal to the total number of RHP poles of $G(s)$ and $K(s)$. It is noteworthy to mention, for this system (see Fig. 3), all the modes of the open-loop systems assumed to be controllable and observable. By analogy (10), which represents the transfer function of source voltage based on terminal voltage of a PEC, is stable if the roots of followed equation have negative real parts:

$$\boldsymbol{det}(\boldsymbol{I} + \boldsymbol{Z_{Sdq}}(\boldsymbol{s}).\boldsymbol{Y_{Ldq}}(\boldsymbol{s})) = \boldsymbol{0}. \tag{12}$$

This condition could be interpreted by Nyquist stability criterion to formulate stability assessment of the PECs during the operational stage by preventing encirclements around point $(-1+0\text{j})$ for the Nyquist diagram of their return-ratio. Furthermore, for the closed-loop systems, it could be utilized in combination with the Middlebrook's stability criterion to formulate GM stability criterion for the PECs. Although, the GM stability criterion is a slightly conservative criterion, it is easier to implement. Basically, it restricts the Nyquist diagram of return-ratio $(\boldsymbol{Z_{Sdq}}(\boldsymbol{s}).\boldsymbol{Y_{Ldq}}(\boldsymbol{s}))$ to lie within the unit circle in the complex plane. In this criterion, only GM of the systems is taken into account regardless of the PM values. Therefore, the stability condition (12), driven from the ac interface of the interconnected source-load PEC, is a general stability condition in the $d-q$ frame that depends on the stability criteria and/or technique may address the stability of the PECs for both pre-operational and operational stages with different degrees of the conservativeness.

Herein, general stability term (12) is measured with the GNC in order to ensure the overall small-signal stability of the system and the results are compared with the GM criterion to illustrate the difference in degree of conservativeness as well as preciseness of the proposed method. Additionally, in order to find a return-ratio matrix of the system in a more convenient manner and in real-time, some legitimate modifications and simplification are considered. In the literature, these simplifications mainly are considered in impedance measurement for high power factor rectifiers [26]–[28].

Generally, the stability at the ac interfaces feeding PECs could be assessed with GNC by applying it to the return-ratio matrix $\boldsymbol{L_{dq}}(\boldsymbol{s})$ where it can be found by

$$\begin{aligned} \boldsymbol{L_{dq}}(\boldsymbol{s}) &= \boldsymbol{Z_{Sdq}}(\boldsymbol{s}).\boldsymbol{Y_{Ldq}}(\boldsymbol{s}) \\ &= \begin{bmatrix} Z_{Sdd} & Z_{\boldsymbol{Sdq}} \\ Z_{Sqd} & Z_{Sqq} \end{bmatrix} . \begin{bmatrix} Y_{Ldd} & Y_{Ldq} \\ Y_{Lqd} & Y_{Lqq} \end{bmatrix} \end{aligned} \tag{13}$$

where $\boldsymbol{Z_{Sdq}}(\boldsymbol{s})$ and $\boldsymbol{Y_{Ldq}}(\boldsymbol{s})$ are, respectively, the source impedance and the load admittance matrices in $d-q$ reference frame. Furthermore, the elements of these matrices in d and q axes are represented in the form of matrix (i.e., Z_{Sdd} is the d-d element of the source impedance matrix or Y_{Ldq} is the $d-q$ element of the load admittance matrix). Note that in the Middlebrook (and also GM) criterion in order to have the systems small-signal stable, components of the return-ratio matrix has to be lied within unit circle. In other words, according to (14) the magnitudes of all the components should be less than unity, regardless of phases, in order to have return ration matrix magnitude not greater than one.

$$|\boldsymbol{L_{dq}}(\boldsymbol{s})| \leq 1 \left| \begin{bmatrix} Z_{Sdd} & Z_{\boldsymbol{Sdq}} \\ Z_{Sqd} & Z_{Sqq} \end{bmatrix} . \begin{bmatrix} Y_{Ldd} & Y_{Ldq} \\ Y_{Lqd} & Y_{Lqq} \end{bmatrix} \right| \leq 1. \tag{14}$$

Therefore, in order to address small-signal stability of such a system via GNC, all the components of the return-ratio matrix should be calculated and addressed. This act is not hard to achieve; however, it increases required computations and will add to the system calculation's complexities. Consequently, some legitimate simplifications and modifications in the method is essential, if the small-signal analysis in real-time is desired.

There have been some studies on stability analysis of the high power factor rectifiers [or more generally converters with power factor correction (PFC)] in which the bode diagram of the load admittance $\boldsymbol{Y_{Ldq}}(s)$ of an AFE converter calculated in connection to the CPL [26]–[28]. The results of these studies are applicable for our model development and they can be utilized for our study since the SST is a power electronics-based device with PFC and comprised from three stages of ac–dc rectifier with PFC, isolated dc–dc bidirectional converter, and a single-phase six-switch inverter. In [26] four elements of bode plot of the load admittance matrix have analyzed and it has been shown that the $d-d$ channel is the only element with negative phase up to the cutoff frequency of the dc bus voltage loop. This means that all the load dynamics represented by load admittance matrix ($\boldsymbol{Y_{Ldq}}(s)$) are reflected on this channel. Therefore, in stability analysis of SST with PFC it is admissible to study $d-d$ element of load admittance matrix for load dynamics. This simplifies (14) and yields lighter computational loads, faster computation times, and more accurate evaluation of the system's stability in a way that enables real-time capability of the proposed method. Consequently, (14) is derived as

$$\begin{aligned}\boldsymbol{L_{dq}}(s) &\approx \begin{bmatrix} Z_{Sdd} & Z_{\boldsymbol{Sdq}} \\ Z_{Sqd} & Z_{Sqq}\end{bmatrix}\cdot\begin{bmatrix} Y_{Ldd} & 0 \\ 0 & 0\end{bmatrix} \\ &\approx \begin{bmatrix} Z_{Sdd}.Y_{Ldd} & 0 \\ Z_{Sqd}.Y_{Ldd} & 0\end{bmatrix} \approx \begin{bmatrix} l_1(s) & 0 \\ l_2(s) & 0\end{bmatrix}. \quad (15)\end{aligned}$$

In addition, it was proven hereinbefore that the small-signal stability at the input terminals of the PECs is determined by the characteristic loci described by the eigenvalues of the corresponding return-ratio matrix $\boldsymbol{L_{dq}}(s)$. Given the input dynamics of the rectifier, the eigenvalues of $\boldsymbol{L_{dq}}(s)$ at the ac interface are given by (15). Consequently, only the eigenvalue associated to the $d-d$ channel [i.e., $l_1(s)$] can actually encircle the critical point ($-1+$ j0), and thus be the cause of instability. The remaining eigenvalue associated to the $q-d$ channel, $l_2(s)$, remains stationary at the origin of the S-plane and thus be incapable of causing instabilities [26]. Therefore, in the proposed method the Nyquist contour of the $l_1(s)$ is determined and examined for the Nyquist evaluation and having the magnitude of the $d-d$ component of the return-ratio matrix less than one, our system is stable [29]. The reason is that if $|l_1(s)|$ is less than one (regardless of its phase), based on (14) it cannot encircle the point ($-1+$ j0) in the s-plane and thus the system is stable. The next crucial step herein is defining $l_1(s)$ in real-time from the systems measurements and information, which can be quite complicated.

B. Real-Time System Identification

To investigate small-signal stability of a PEC in real-time, some practical considerations and model simplification are required. The model simplification was discussed in the prior section by considering the $d-d$ channel component of the return-ratio matrix instead of the entire matrix. The practical considerations of the proposed method are:

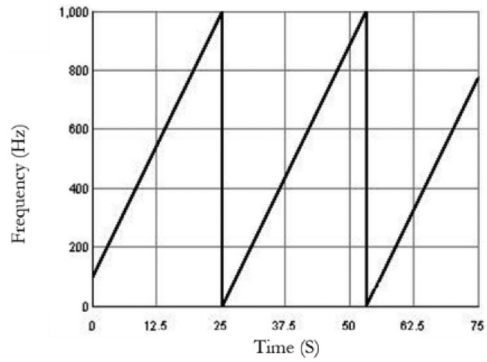

Fig. 5. Chirp excitation signals (swept-sine signals) in order to enable real-time capability.

1) Perturbing the system with the chirp signal, $x(t)=A\sin(2\pi(f_0+(f_1-f_0)\,t/2T)t))$, this helps the real-time capability and nonlinearity consideration simultaneously. Where$x(t)$ could be the voltage and/or current signal, depending on the type of perturbation (series voltage and/or shunt current), A is the magnitude of the perturbation, f_0 is the start frequency, f_1 is the end frequency, and T is the duration of the chirp signal (for real-time applications, the chirp signal is periodic and T should be reset after reaching final value). Following is the graph of frequency change based on the time. As it is depicted in Fig. 5, the frequency reset happens at 27 s.
   Utilizing chirp signals to perturb a system for impedance measurement purposes facilitates perturbation of the system in a range of frequencies and in real-time simultaneously. In other techniques, in order to be able to perturb systems in a range of frequencies, the test system must be perturbed separately at each single frequency, thus preventing those techniques to be applicable for real-time applications.
2) Perturbing the system at source interface as well as load interface at the same time; this helps to gather all the required data for the impedance measurements in real-time and without interference.
   The procedure of the proposed real-time small-signal stability assessment method is described as follows:
   a) acquiring required information to calculate source and load impedances [based on (3)–(6)] in a PEC by measuring voltages and currents in the source and load sides of it as well as perturbation signals;
   b) defining source impedance and load admittance by $d-q$ impedance measurement theory described in Section II;
   c) transforming source impedance and load admittance from time domain to frequency domain by employing FFT;
   d) after defining source and load impedances in frequency domain and based on (5), it is possible to calculate return-ratio matrix (production of source impedance and load admittance).

By having the return-ratio matrix in frequency domain, it is possible to identify generalized Nyquist contour of the $d-d$ component. Subsequently, small-signal stability can be addressed by utilizing GNC theorem described in Section II.

IV. Offline Stability Analysis

The major advantage of the proposed approach in the previous section is its ability to detect the instability during online operation of the system. However, in many practical applications we are also interested to know about the stability limits of the component before putting it online to avoid operating it in conditions that can threaten the stability of the entire system. Therefore, in this section based on the impedance measurement technique, we provide an offline analysis approach, which is capable of determining the stability conditions for PECs, and thus complements the online approach. The online approach was based on Nyquist criterion. The Nyquist criterion can tell whether the closed loop system has poles in the RHS or not, and thus determine the stability of the system without providing information about the exact location of the closed loop poles. As in offline analysis we have more computational resources, it is advantageous to directly look into the poles of the closed-loop system and analyze how they change as a function of system parameters such as changes in the loading conditions. This enables us to have a thorough understanding of the behavior of the system and determine its stability region in terms of different system parameters.

A. Offline System Identification

The first step in analyzing the system's stability in the offline approach is to identify the small-signal dynamics of the system. Based on (2), the transfer function from the source voltage to the load voltage is given as

$$\boldsymbol{T}(s) = (\boldsymbol{I} + \boldsymbol{Z_{Sdq}}(s).\boldsymbol{Y_{Ldq}}(s))^{-1}. \tag{16}$$

This transfer function consists of two matrices: $\boldsymbol{Z_{Sdq}}(s)$ and $\boldsymbol{Y_{Ldq}}(s)$. The first matrix, $\boldsymbol{Z_{Sdq}}(s)$, depends on the dynamics of the PEC, which needs to be identified. We will use bode plots of the elements of this matrix for its identification. The second matrix, $\boldsymbol{Y_{Ldq}}(s)$, depends on the value of the load and is the part of the system which depends on the loading conditions. If this load is shown by $R + jL\omega_e$, where ω_e is the frequency of the system, then in the single phase $d-q$ transform, $\boldsymbol{Z_{Ldq}}(s)$ can be written as [30]

$$\boldsymbol{Z_{Ldq}} = \begin{bmatrix} R+Ls & -L\omega_e \\ L\omega_e & R+Ls \end{bmatrix}. \tag{17}$$

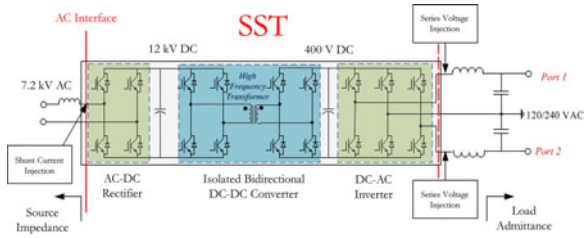

Fig. 6. Schematic of a SST used as a sample PEC with perturbations in source and load interfaces simultaneously (in order to enable real-time capability).

B. Finding the Eigenvalues of the System

Once $\boldsymbol{Z_{Sdq}}(s)$ is identified, a parametric expression for the eigenvalues can be found where the parameters depend on the values of *R* and *L*. The eigenvalues of the system would be the poles of the transfer function given in (16), which would be the roots of

$$\det(I + \boldsymbol{Z_{Sdq}}(s)\boldsymbol{Y_{Ldq}}(s)) = 0. \tag{18}$$

For instance if $Z_{\boldsymbol{Sdq}}(\mathrm{s})$ is a constant gain, then the roots of (18) would be as (19) as shown bottom of the page, where

$$\boldsymbol{Z_{Sdq}} = \boldsymbol{K} = \begin{bmatrix} k_1 & k_2 \\ k_3 & k_4 \end{bmatrix}. \tag{20}$$

In this case, the system would be stable if $\mathrm{Re}(s_1) < 0$, and $\mathrm{Re}(s_2) < 0$.

V. Case Study

A. Case Study Setup

In this section, the small-signal stability of a sample PEC is studied and well-discussed for asymptotic stable, marginally stable and unstable conditions. An SST connected to the source and load (see Fig. 6) is used to represent a sample PEC. First, the results of the online approach using the impedance measurement-based method utilizing unit circuit criterion are presented. To illustrate the capability of the proposed technique to address the small- signal stability of the systems, all three possible types of stability (asymptotic, marginal, and unstable) are studied within the test system. To this end, three different loading conditions are instantiated for each type of stability. Next, using the proposed offline procedure, the stability region of the PEC in terms of the loading conditions is determined which is in agreement with the results of the online approach.

$$\begin{aligned} s_1 &= -\frac{1}{2L}\left(2R + k_1k_4 + \sqrt{4k_2k_3 - 2k_1k_4 - 4L^2\omega_e^2 + k_1^2 + k_4^2 + 4L\omega_e k_2 - 4L\omega_e k_3}\right) \\ s_2 &= -\frac{1}{2L}\left(2R + k_1k_4 - \sqrt{4k_2k_3 - 2k_1k_4 - 4L^2\omega_e^2 + k_1^2 + k_4^2 + 4L\omega_e k_2 - 4L\omega_e k_3}\right) \end{aligned} \tag{19}$$

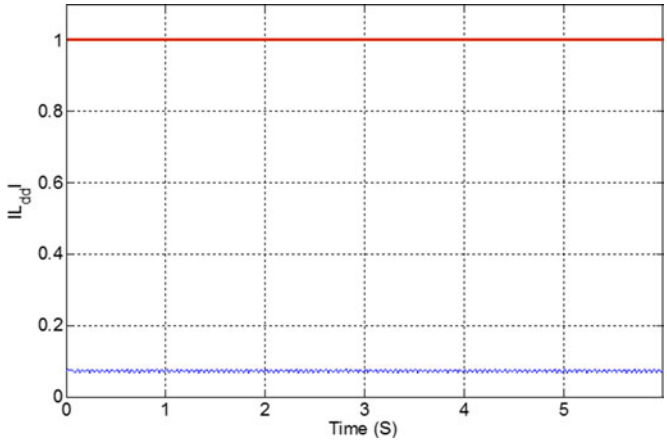

Fig. 7. Online stability metric showing the relative stability of the test bed for asymptotic stability.

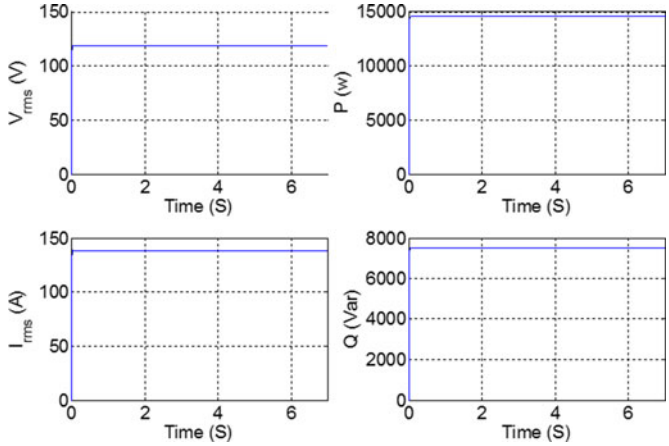

Fig. 8. Simulation results in time-domain for the stable test system: (a) and (b) RMS voltage and current in LV; (c) and (d) active and reactive powers.

B. Real-Time Stability Analysis Results in RTDS Platform

In order to study the proposed technique for real-time applications, a new test system is developed in RTDS. In addition, in order to verify the proposed technique, the average value model of an SST [31] is utilized in the abovementioned test system. The STT model, as well as all the required blocks to achieve return-ratio matrix in real-time, are developed in the RTDS. One of the most significant advantages of the proposed stability technique over other developed techniques is its real-time capability. This capability is enabled by utilizing chirp signal excitation and parallel perturbations (discussed in Section III-B) in the proposed technique and employing RTDS to develop the test system and stability technique in real-time. Fig. 6 depicts a standard ac interface of a SST; where the current injections (perturbations) and measurements are taken place.

Utilizing chirp signal to perturb systems for impedance measurement purposes facilitates system perturbations in a range of frequencies and in real-time simultaneously. In other techniques, in order to be able to perturb systems throughout a range of frequencies, the test system must be perturbed for each single frequency thus preventing those techniques to be applicable for real-time applications. Furthermore, parallel perturbations facilitate the data acquisition process for source impedance and load admittance concurrently.

1) System With Asymptotic Stability: In order to validate the method in the stable conditions, a single phase SST is connected to the ideal source from primary side and a *RL* load is connected to the secondary side of the SST (port 1 and 2 in Fig. 6). The high-voltage and low-voltage levels of the SST are 7.2 (kV) and 120 (V), respectively, and 1.534 + j0.753 (Ω) is the initial load of the system. Magnitude of the $d-d$ component for the return-ratio matrix $[l_1(s)]$ is illustrated in Fig. 7. Based on Nyquist evaluation the system is stable in this loading condition since $|l_1(s)|<1$ and the Nyquist contour does not encircle point $-1+0$j. It is also possible to address relative stability of the systems based on the distance between unit circle stability criterion and line $y=1$. In this test, the system is far away from instability margin, since the magnitude of the $l_1(s)$ component of the return-ratio matrix is significantly less than 1. Fig. 8 shows the RTDS simulation results for RMS voltage, current, and active and reactive powers. These results reveal that our system is stable in this condition due to the convergence of active and reactive powers as well as consistence voltage and current values.

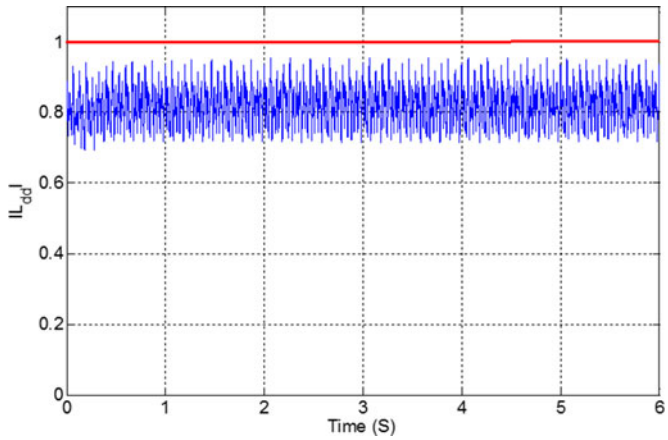

Fig. 9. Online stability metric for the marginal stable test system.

2) System With Marginal Stability: To further study how the proposed stability technique behaves in sensitive and critical situations, the *R* and *L* values connected to the test system is reduced to 10% of its initial value and the system has run again. In other words, for the new test scenario we increased the load of our system by the factor of 10 since the SST provides regulated output voltage and we decreased the impedance by 10%. The marginal stability condition in the proposed technique and with the unit circle criterion may be interpreted by the magnitude of the $d-d$ component in the return-ratio matrix, $l_1(s)$. In other words, the system is marginally stable while $|l_1(s)|=1$.

Fig. 9 shows the magnitude of the $l_1(s)$ component of return-ratio matrix. Although $l_1(s)$ does not pass critical line of $y=1$, its magnitude is close enough to one that it can be interpreted as

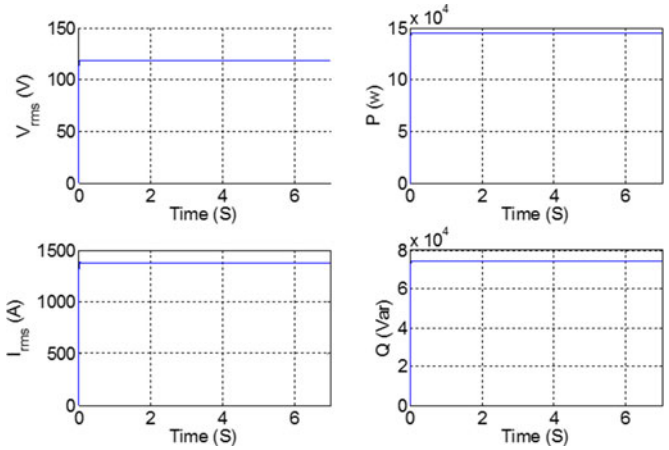

Fig. 10. Simulation results in time-domain for marginally stable test system: RMS voltage and current in LV of SST; active and reactive powers.

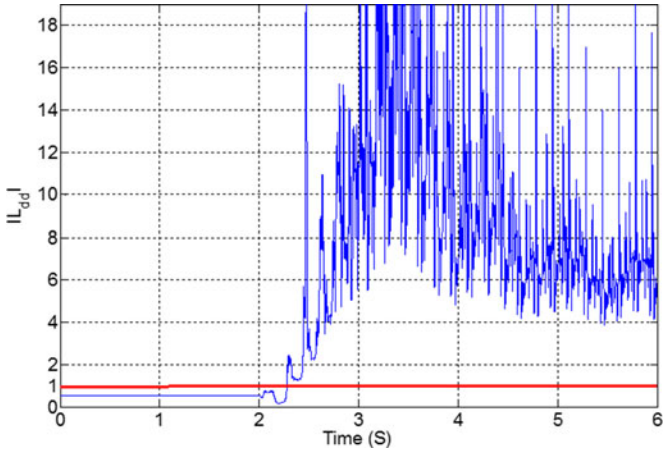

Fig. 11. Stability metric (unit circuit stability criterion) showing the test system becoming unstable.

a marginal stability based on generalized Nyquist and relative stability concepts.

On the other hand, Fig. 10 shows the RTDS simulation results for this case in time-domain. As it is shown, in this case the RMS values of current and voltage of the SST are constant and also the output powers have converged which verifies the stability of the system in this loading condition (even though the system is one step away from becoming unstable).

A simple comparison between experiments 1 and 2 shows that it is not possible to distinct the systems' stability conditions from their time-domain data and before becoming unstable; however, with the proposed stability criterion it is possible to find the relative stability condition of the systems and take precautionary measures before the systems become unstable.

3) Small-Signal Stability Analysis of the Test Bed by Gradual Decrement in Load That Cause Instability: As described above, based on GNC, a system is unstable when the Nyquist contour of the return-ratio matrix encircles point –1 + 0j. This fact can be interpreted by the unit circle criterion that the magnitude of the return-ratio is greater than 1. In this test case, the *R* and *L* values connected to the SST are gradually decreased to 1% of their initial value while the system is operating. Based on what we have discussed before, the output voltage of the SST is regulated and by decreasing the value of impedance, we will increase the load current and as a result the actual load of the system. Therefore, in this test we gradually increased the load of the system from initial value (in Section I) to analyze its behavior while becoming unstable. This gradual change in the load is made by a slider connected to the variable *RL* load in the model and it causes instability of the system after almost 2.2 (s). The system's stability status is monitored in real-time and the results are saved and shown below. As shown in Fig. 11 the magnitude of the $d-d$ channel of the return-ratio matrix, $\mathrm{l}_1\,(\mathrm{s})$, exceeds the critical line $y=1$ in almost 2.2 (s) due to the change in the loading condition of the test bed. In fact, it can be seen that the system's instability in the time-domain occurs simultaneously with crossing the $|\mathrm{l}_1\,(\mathrm{s})|$ loci and line $y=1$.

This fact is also shown in Fig. 12 by illustrating the RMS values for the voltage, current, active, and reactive powers. This

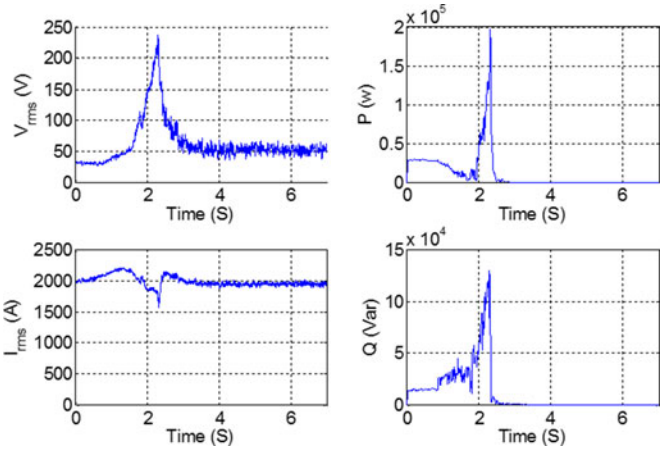

Fig. 12. Simulation results in time-domain for the unstable test system: (a) and (b) RMS voltage and current in LV side of the SST; (c) and (d) active and reactive powers.

figure clearly depicts that complete instability, due to the system breakdown, occurs after approximately 2.2 (s) of simulation and as a result of change in *R* and *L* values during the real-time simulation.

C. Offline Stability Analysis

Using the same impedance measurement technique used in the online approach, the bode plots of Fig. 13 are found for $\boldsymbol{Z_{Sdq}}\,(s)$, where

$$\boldsymbol{Z_{Sdq}} = \begin{bmatrix} Z_{Sdd} & Z_{\boldsymbol{Sdq}} \\ Z_{Sqd} & Z_{Sqq} \end{bmatrix}. \tag{21}$$

From the bode plots, we can see that all the phases are around zero and the magnitudes are almost constant for all the frequencies. This suggests $\boldsymbol{Z_{Sdq}}\,(s)$ is a constant gain given by

$$\boldsymbol{Z_{Sdq}} = \begin{bmatrix} 0.198 & 0.186 \\ 0.281 & 0.250 \end{bmatrix}. \tag{22}$$

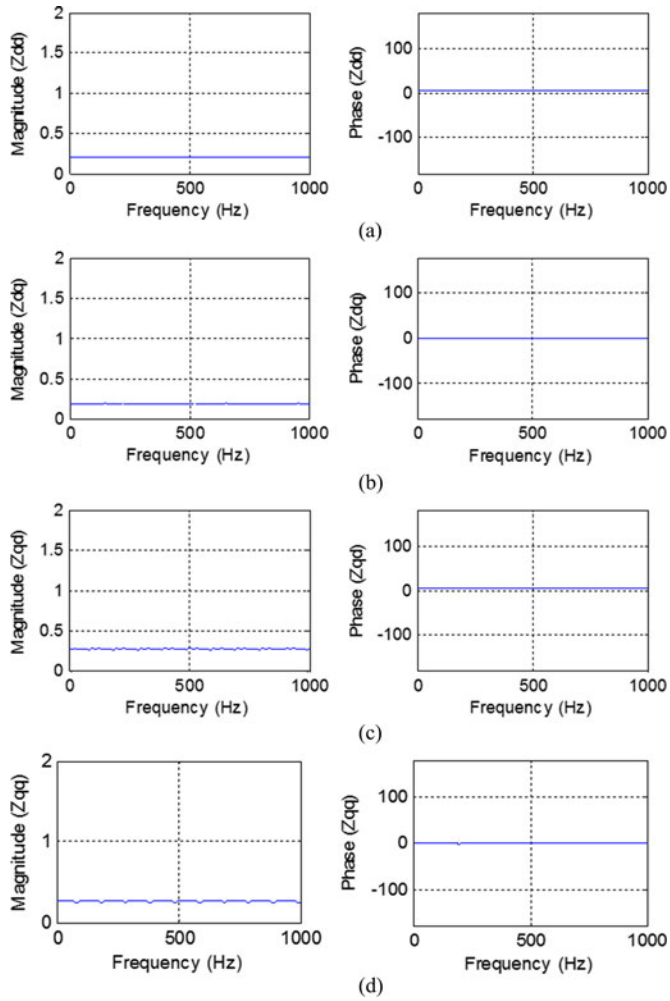

Fig. 13. Bode plots for (a) $Z_{\boldsymbol{Sdq}}(s)$, (b) $Z_{Sdd}(s)$, (c) $Z_{Sqd}(s)$, $Z_{Sqq}(s)$.

Now, based on (19), it is evident that real part of S_1 is always negative. Therefore, stability depends only on S_2. So the stability condition would be (23), as shown bottom of the page, where

$$\begin{bmatrix} k_1 & k_2 \\ k_3 & k_4 \end{bmatrix} = \begin{bmatrix} 0.198 & 0.186 \\ 0.281 & 0.250 \end{bmatrix}. \tag{24}$$

Remark: To do the offline analysis, we have used the same data measured in online experiments. The bode plots in Fig. 13, are the identified $d-q$ impedances on the source side for the SST used in the entire experiments. The $d-q$ impedances at the source side are not the choice of authors but they are the result of the identification process. The results indicate that from the source side, $d-q$, the SST acts like a constant gain under different loading conditions.

Based on (23), the stability region of the system can be found by evaluating *v* at different value of *R* and *L*. The stability region is drawn in Fig. 14. The x-axis is the value of R, and the y-axis is

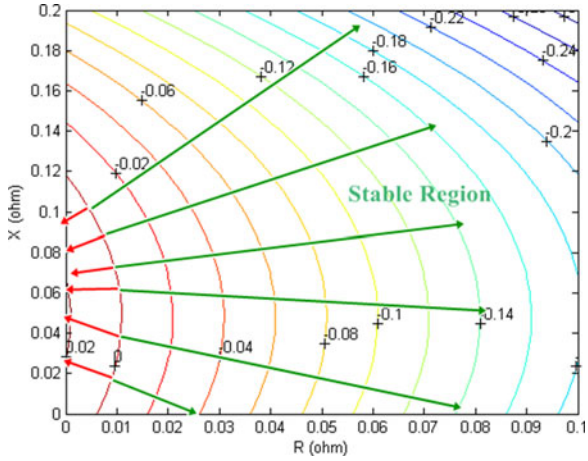

Fig. 14. Stability region of the system as a function of *R* and *X*.

the value of $X = Lw$. The lines are the contours of *v* [as defined in (23)] and the numbers on the lines determine the value of *v* along that line. The stability region is marked as the region where the values of all the contours are positive and it is marked with green arrows. The unstable region is marked with red arrows and forms a small portion of the loading condition of the system. As the values of *R* and *L* decrease, the loading of the system increases and after a certain limit, the system enters the unstable region. This limit encompasses all the values along the contour $v = 0$. This trend is in agreement with the simulation results in RTDS as well as the online stability analysis approach. In fact, the values of *R* and *L* for which the online stability approach detects stability fall inside the stable region in Fig. 14.

VI. Hardware Development and Experimental Implementation

In this section, the small-signal stability of a SST is investigated through PHIL experiment [32]. For this, an average value model of an SST [31] is developed in the RTDS platform and the last stage of the SST (six-switch, single-phase inverter) connected to the variable ac load is implemented in hardware. Subsequently, the small-signal stability of the test system is investigated during load variation via programmable ac load. Fig. 15 demonstrates the hardware development part for this experiment.

The primary reason for this experiment is to investigate small-signal stability of an SST during different loading condition and operating points. Since the full SST in hardware was not available to conduct the experiment, we decided to implement this experiment through PHIL method. Generally, in PHIL experiment some part of a system is modeled in a real-time simulator (i.e., RTDS) and the rest is developed in hardware. These two parts of PHIL, simulation and hardware, are communicating to

$$v = \mathrm{Re}\left(2R + k_1 + k_4 - \sqrt{4k_2k_3 - 2k_1k_4 - 4L^2\omega_e^2 + k_1^2 + k_4^2 + 4L\omega_e k_2 - 4L\omega_e k_3}\right) < 0 \tag{23}$$

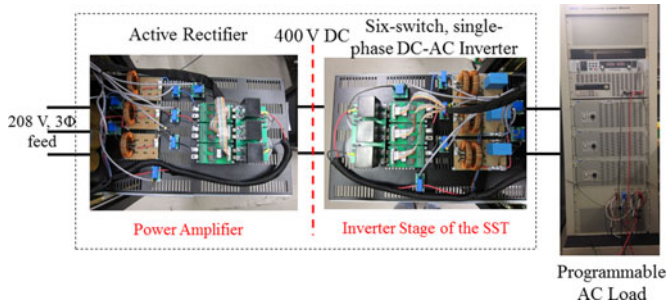

Fig. 15. Developed hardware for the proposed PHIL experiment to emulate the last stage of the SST connected to programmable ac load.

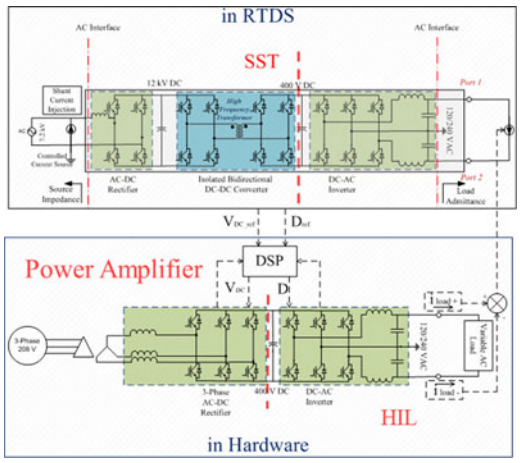

Fig. 16. Schematic of the developed PHIL experiment to study small-signal stability of a SST in real-time and during load variation.

each other though their interfaces and transferring the data in order to control the system [32]. The PHIL experiment shown in Fig. 16 explains the IMU implementation allowing for the small-signal stability of the developed test system to be assessed.

As is shown in Fig. 16, the dc voltage reference from RTDS is employed in the PI controller to emulate the input dc voltage of the inverter in the test bed. Furthermore, the inverter utilizes duty-cycles (Ds) references for switching, enabling the test bed to emulate voltage waveforms at the inverter terminals identical to the RTDS model.

In the developed PHIL experiment the dc link voltage (inverter input) and the inverter Ds signals are sent via RTDS analog output (GTAO) to hardware controller (TI-eZdsp F28335) and are utilized to control the hardware in the way that emulates the last stage of the SST. All three signals sent from RTDS to hardware controller (DSP) as references are captured after digital-to-analog converter (DAC) by scope and are shown in Fig. 17.

Moreover, the communication between RTDS analog output (DAC) in the simulator lab [see Fig. 18(a) and (b)] and DSP IoCU board analog inputs [see Fig. 18(c)] has been done with the fiber optic cable that connects simulator lab to the hardware controllers in the labs.

The implemented hardware for this experiment is shown in Fig. 19. The main stages of the system are three-phase

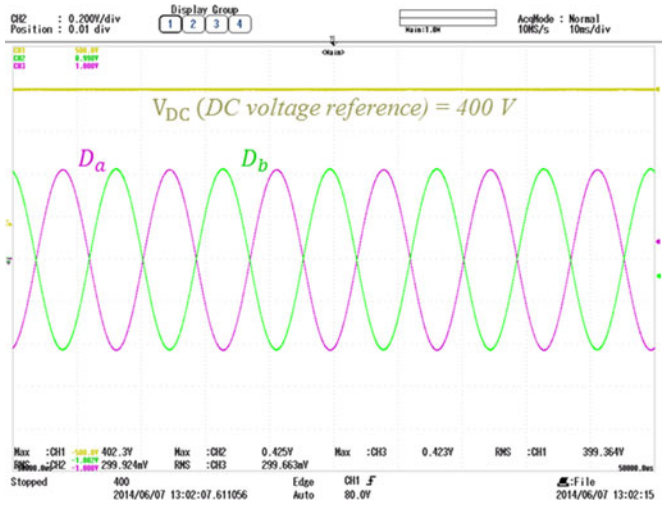

Fig. 17. Dc voltage and duty cycles are used as references from RTDS to DSP.

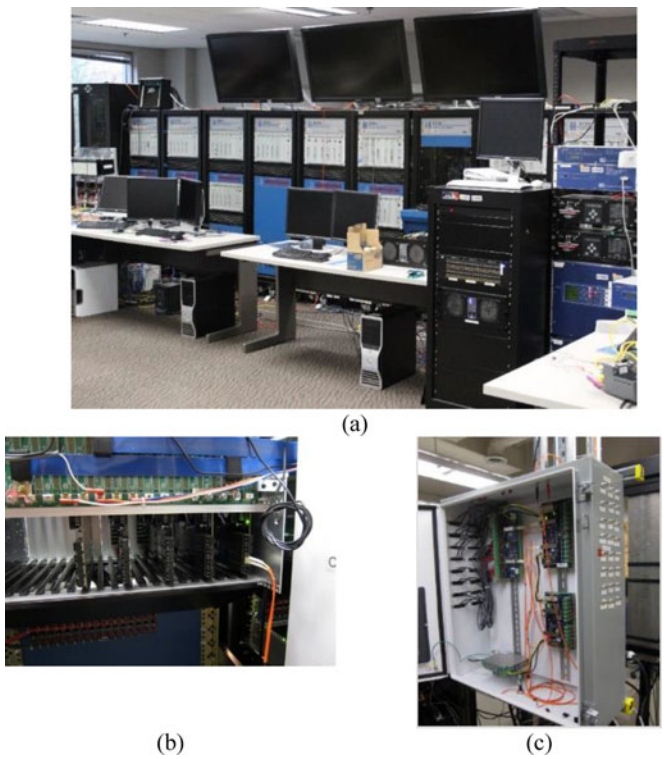

Fig. 18. (a) Simulator lab at Florida State University Center for Advanced Power Systems. (b) DAC card at the back of the RTDS rack. (c) DSP IoCU board analog inputs and outputs.

transformer, three-phase two-level boost rectifier, test bed controller, and six-switch single-phase inverter. The three-phase boost rectifier provides the power for the inverter on the dc link of its output capacitor (see Fig. 16). Therefore, it is utilized as the power amplifier stage for the test bed and thus this experiment is called PHIL [instead of hardware-in-the-loop (HIL) or control HIL (CHIL)].

As was mentioned hereinbefore, in the proposed hardware development experiment, loading the test system under different conditions is one of the significant reasons that might push

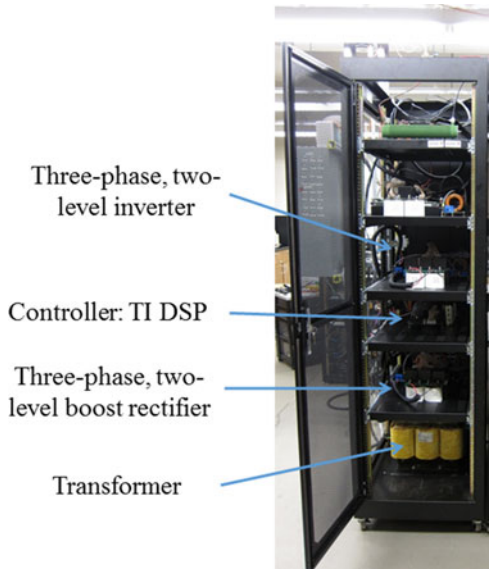

Fig. 19. Implemented hardware in the lab for the proposed PHIL experiment to study small-signal stability of an SST in real time.

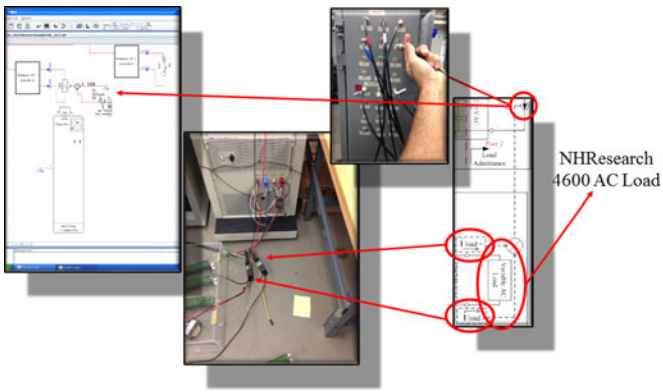

Fig. 20. Measuring and feeding back the current to the real-time model through RTDS analog input interface (GTAI).

the test system into an unstable region of operation. Therefore, as is shown in Fig. 15 the inverter output is connected to the programmable ac load (NHR 4600 ac load) to change the SST load and study small-signal stability of the SST during load variation in real-time. In addition, the output voltage of the SST is fixed (due to its regulated output voltage characteristic); thus, changes in the programmable ac load will affect the load current. Consequently, in order to assess the test system under different loading conditions, the load current must be fed back to the RTDS. This also is accomplished by measuring the load current with the current probes and sending it to the RTDS analog input interface (GTAI) via fiber optic and implement it in the model with the variable current source. Fig. 20 demonstrates different stages of this section such as measuring the signals with probes and using RTDS analog input interface (GTAI) to feed back the measured signals to the real-time model.

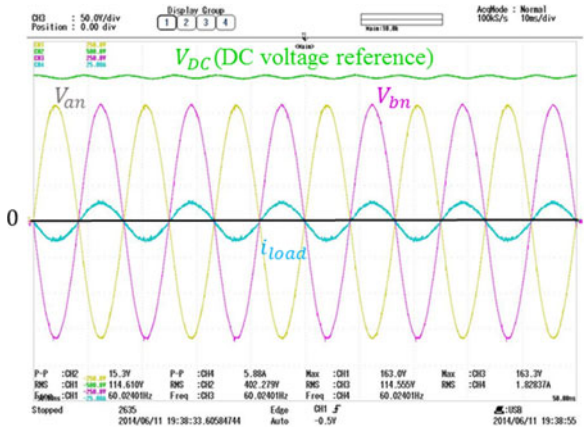

Fig. 21. Inverter input (dc), output (ac) voltages, and load current for constant *RL* load test.

A. Open-Loop Test With Constant RL Load

For the development of above described PHIL experiment, the first stage was to perform an open-loop, no-load test. This step basically compared experimental voltage waveforms with those from the developed model RTDS platform and the output voltage of the inverter in the test system. The second step is an open-loop test by connecting the load terminals to the simple *RL* load. This step has been done by connecting the output terminals of the inverter to the load with $R = 132\,\Omega$ and $L = 1\,\text{mH}$. Fig. 21 depicts the input dc voltage, output ac voltages, and load current for this experiment. As is depicted, dc voltage is almost 400 (V) with less than 3.7% ripple. The RMS load current is 1.82 (A). The RMS ac voltage across the load is almost 228 (V).

B. Closed-Loop Test With Programmable AC Load and Load Increment

The experiment described in Section VI-A was an open-loop test. In this study, open-loop means that there is not any feedback from the test bed back to the simulated model in RTDS. An open-loop test has been conducted to check the test bed settings/configuration by comparing the results with simulation results. As a final step, a close-loop test and PHIL experiment will be performed. Closed-loop tests are actually necessary for PHIL experiments for the reason that there should be feedback from test bed to the simulated model in order to complete a PHIL experiment. This feedback is what makes the test system closed-loop. At this section, the close-loop test that has been done with the NHR 4600 programmable ac load and the stability of the test system under different loading condition is investigated in real-time and through a PHIL experiment. Different stages of this PHIL development is as follows:

1) the RTDS model of the SST runs in real-time and the dc voltage and duty cycles are sent to the DSP (controller);
2) the DSP utilizes above-mentioned signals as references to emulate the last stage of the SST (inverter) in the test bed;

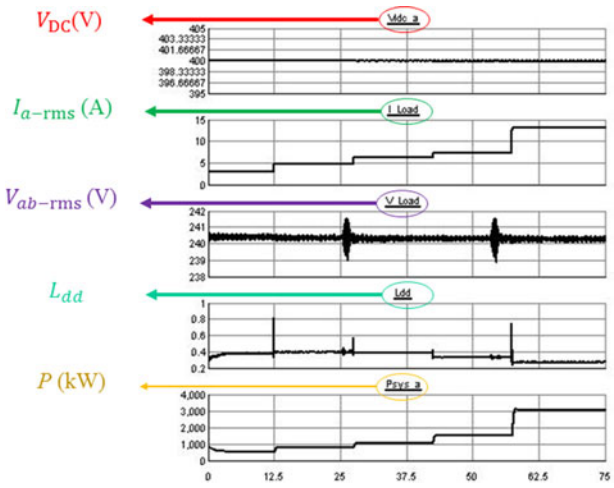

Fig. 22. PHIL experiment results captured in RTDS.

3) output terminals of the two-level three-leg inverter are connected to the single-phase ac programmable load;
4) the ac load is increased, the load current is measured via probe, the probe signal (load current) is sent to the RTDS and applies to the controlled-current source;
5) controlled-current source in the RTDS model performs in a way that represents ac programmable load is in the model and changes;
6) the results captured in RTDS and stability criterion (L_{dd}) is computed and shown.

Simulation results for all the incremental steps in the load are also captured and illustrated together in Fig. 22. This PHIL experiment was conducted for almost 120 s, and as can be observed in the figure, the data were collected for 75 s. This 75 s period was divided into five 15-s parts, where the ac load was changed to 0.5, 0.75, 1, 1.5, and 3 (kW), respectively, for each period. The first graph in Fig. 22 shows the dc voltage link (AFE output) during this experiment. As can be seen, the dc link is held constant at 400 (V) with ripple. The dc voltage ripples are boosted by load increments at the output of the inverter. This fact is expected as characteristics of the single-phase inverter. For a single-phase inverter if instantaneous power changes as a function of time the input dc voltage ripple is expected. The second and third graph illustrate the RMS load current and load voltage transitions for this experiment. The RMS load current values are identical with the values from scope captures. The RMS load voltage remains constant at around 240 (V), since the voltage feedback has been used in the SST to have constant output voltage. The ripple for the voltage is a result of the perturbations with the series voltage injection source. It can be observed that the ripples are higher when the perturbations are closer to 1 (kHz) frequency. The fourth graph shows the magnitude of the $d-d$ channel of return-ratio matrix. As it was well-discussed in Section IV, L_{dd} may be used for the small-signal analysis with the unit circle criterion. For stable systems, this value is less than unity. Therefore, the test system is stable for all the loading conditions in this experiment. The last graph depicts the active power transition for this test.

VII. Conclusion

The stability analysis of the PEC based distribution systems is challenging because the system dynamics change with the loading conditions. This paper proposed two approaches of real-time and offline techniques to overcome this challenge based on small-signal impedance measurement. In the real-time approach, the system's dynamics are identified in real-time and based on Nyquist stability criterion, the stability of the system is assessed in different loading conditions while system operates. This approach, not only can detect the unstable conditions while the system is operating, but also it can identify the system's relative stability based on the stability criterion's distance to instability margin. In the offline approach, the constant part of the system is identified offline and based on the eigenvalue analysis, a stability region is found for the system as a function of loading conditions. This approach demarcates the stability limits of the component before putting it online to avoid operating it in conditions that can threaten the stability of the entire system. Both approaches are validated on an SST based circuit which is simulated on an RTDS. As final demonstration of the proposed real-time technique, hardware development and experimental implementation are discussed and small-signal stability of SST was assessed through development of PHIL experiment. For the PHIL experiment, an IMU was developed partially in the RTDS platform and the rest in an actual hardware test bed. Subsequently, stability of SST was investigated through the PHIL experiment by implementing the final inverter stage of the SST into the test bed and loading the SST with the programmable ac load. The magnitude of the ac load connected to the SST was changed and the stability criterion of the test system was analyzed, along with the voltages/currents/power waveforms.

References

[1] H. E. Z. Farag, E. F. El-Saadany, and R. Seethapathy, "A two ways communication-based distributed control for voltage regulation in smart distribution feeders," *IEEE Trans. Smart Grid*, vol. 3, no. 1, pp. 271–281, Mar. 2012.
[2] A. Q. Huang, M. L. Crow, G. T. Heydt, J. P. Zheng, and S. J. Dale, "The future renewable electric energy delivery and management (FREEDM) system: The energy internet," *Proc. IEEE*, vol. 99, no. 1, pp. 133–148, Jan. 2011.
[3] A. Mnatsakanyan and S. W. Kennedy, "A novel demand response model with an application for a virtual power plant," *IEEE Trans. Smart Grid*, vol. 6, no. 1, pp. 230–237, Jan. 2015.
[4] M. A. Salmani, S. M. M. Tafreshi, and H. Salmani, "Operation optimization for a virtual power plant," in *Proc. IEEE Sustainable Alternative Energy Conf.*, 2009, pp. 1–6.
[5] M. A. Salmani, S. M. M. Tafreshi, and A. Bagherian, "Virtual power plant: Concept and operation optimization algorithm," *J. Int. Rev. Electr. Eng.*, vol. 5, pp. 2271–2279, 2010.
[6] R. Effatnejad, H. Salmani, M. A. Salmani, and H. Modirzare, "Virtual power plant (VPP) and economic dispatch (ED)," *Int. J. Phys. Sci.*, vol. 47 , pp. 6117–6129, 2012.
[7] N. Rahbari-Asr, U. Ojha, Z. Zhang, and M.-Y. Chow, "Incremental welfare consensus algorithm for cooperative distributed generation/demand response in smart grid," *IEEE Trans. Smart Grid*, vol. 5, no. 6, pp. 2836–2845, Nov. 2014.
[8] N. Rahbari-Asr and M.-Y. Chow, "Cooperative distributed demand management for community charging of PHEV/PEVs based on KKT conditions and consensus networks," *IEEE Trans. Ind. Inform.*, vol. 10, no. 3, pp. 1907–1916, Aug. 2014.

[9] M. Belkhayat, R. Cooley, and A. Witulski, "Large signal stability criteria for distributed systems with constant power loads," in *Proc. Power Electron. Spec. Conf.*, 1995, pp. 1333–1338.
[10] H. Saadat, *Power System Analysis*. New York, NY, USA: McGraw-Hill, 2011.
[11] J. Gerlof Slootweg, "Wind power modeling and impact on power system dynamics," Ph.D. Dissertation, TU Delft, Dept. of Elect. Eng. Delft, The Netherlands, 2003.
[12] B. P. Loop, S. D. Sudhoff, S. H. Zak, and E. L. Zivi, "Estimating regions of asymptotic stability of power electronics systems using genetic algorithms," *IEEE Trans. Control Syst. Technol.*, vol. 18, no. 5, pp. 1011–1022, Sep. 2010.
[13] N. Bottrell, M. Prodanovic, and T. C. Green, "Dynamic stability of a microgrid with an active load," *IEEE Trans. Power Electron.*, vol. 28, no. 11, pp. 5107–5119, Nov. 2013.
[14] S. D. Sudhoff and S. F. Glover, "Modeling techniques, stability analysis, and design criteria for DC power systems with experimental validation," *SAE Trans. J. Aerospace*, Section 1, pp. 52–67, 1998.
[15] N. Pogaku, M. Prodanovic, and T. C. Green, "Modeling, analysis and testing of autonomous operation of an inverter-based microgrid," *IEEE Trans. Power Electron.*, vol. 22, no. 2, pp. 613–625, Mar. 2007.
[16] G. O. Kalcon, G. P. Adam, O. Anaya-Lara, S. Lo, and K. Uhlen, "Small-signal stability analysis of multi-terminal VSC-based DC transmission systems," *IEEE Trans. Power Syst.*, vol. 27, no. 4, pp. 1818–1830, Nov. 2012.
[17] Y. Berkovich and A. Ioinovici, "Large-signal stability-oriented design of boost regulators based on a Lyapunov criterion with nonlinear integral," *IEEE Trans. Circuits Syst. I: Fundam. Theory Appl.*, vol. 49, no. 11, pp. 1610–1619, Nov. 2002.
[18] S. R. Sanders and George C. Verghese, "Lyapunov-based control for switched power converters," *IEEE Trans. Power Electron.*, vol. 7, no. 1, pp. 17–24, Jan. 1992.
[19] J. Sun, "Impedance-based stability criterion for grid-connected inverters," *IEEE Trans. Power Electron.*, vol. 26, no. 11, pp. 3075–3078, Nov. 2011.
[20] M. A. Salmani and C. S. Edrington, "Real-time small signal stability analysis of the power electronic-based components in contemporary distribution systems," *Electr. Power Syst. Res. J.*, vol. 117, pp. 47–58, 2014.
[21] Y. A. Familiant, J. Huang, K. A. Corzine, and M. Belkhayat, "New techniques for measuring impedance characteristics of three-phase AC power systems," *IEEE Trans. Power Electron.*, vol. 24, no. 7, pp. 1802–1810, Jul. 2009.
[22] M. Belkhayat, "Stability criteria for AC power systems with regulated loads," Ph.D. Dissertation, Dept. of Elect. Eng. Purdue Univ., West Lafayette, IN, USA, Dec. 1997.
[23] R. D. Middlebrook, "Input filter considerations in design and application of switching regulators," in *Proc. IEEE Ind. Appl. Soc. Conf.*, 1976, pp. 366–382.
[24] B. Wen, D. Boroyevich, R. Burgos, P. Mattavelli, and Z. Shen, "Small-signal stability analysis of three-phase AC systems in the presence of constant power loads based on measured D-Q frame impedances," *IEEE Trans. Power Electron.*, vol. 30, no. 10, pp. 5952–5963, Oct. 2015.
[25] H. Wang, W. Mingli, and J. Sun, "Analysis of low-frequency oscillation in electric railways based on small-signal modeling of vehicle-grid system in dq frame," *IEEE Trans. Power Electron.*, vol. 30, no. 9, pp. 5318–5330, Sep. 2015.
[26] R. Burgos, D. Boroyevich, F. Wang, K. Karimi, and G. Francis, "Ac stability of high power factor multi-pulse rectifiers," in *Proc. Energy Convers. Congr. Expo.*, 2011, pp. 3758–3765.
[27] J. Sun, M. Chen, and K. J. Karimi, "Aircraft power system harmonics involving single-phase PFC converters," *IEEE Trans. Aerospace Electron. Syst.*, vol. 44, no. 1, pp. 217–226, Jan. 2008.
[28] Z. Bing, K. J. Karimi, and J. Sun, "Input impedance modeling and analysis of line-commutated rectifiers," *IEEE Trans. Power Electron.*, vol. 24, no. 10, pp. 2338–2346, Oct. 2009.
[29] M. A. Salmani and C. S. Edrington, "Small-signal stability assessment of the power electronic-based AC systems using impedance measurement-based technique," in *Proc. North Amer. Power Symp.*, 2013, pp. 1–6.
[30] P. Xiao, G. Venayagamoorthy, and K. Corzine, "A novel impedance measurement technique for power electronic systems," in *Proc. Power Electron. Spec. Conf.*, 2007, pp. 955–960.
[31] T. Zhao, J. Zeng, S. Bhattacharya, M. E. Baran, and A. Q. Huang, "An average model of solid state transformer for dynamic system simulation," in *Proc. Power Energy Soc. General Meeting*, 2009, pp. 1–8.
[32] A. Benigni and A. Monti, "A parallel approach to real-time simulation of power electronics systems," *IEEE Trans. Power Electron.*, vol. 30, no. 9, pp. 5192–5206, Sep. 2015.

Mohamadamin Salmani (M'13) received the B.S. and M.S. degrees in power electrical engineering from the K. N. Toosi University of Technology, Tehran, Iran, in 2006 and 2009, respectively. In 2011, he joined the Center for Advanced Power Systems (CAPS), Florida State University (FSU), Tallahassee, FL, USA, to work toward the Ph.D. degree in electrical engineering with concentration in power systems and power electronics. He received the Ph.D. degree from FSU in 2014.

He has worked at the Iran Power Plant Projects Management Company from 2009 till 2011 as a Senior Electrical Engineer in the Investment Project Division. Since 2015, he has worked as a Postdoctoral Research Scholar at CAPS in the area of high-temperature superconducting cables. His research interests include power electronics and drives, power systems analysis and control, and applications of power electronics apparatus in distribution systems and smart grids.

Navid Rahbari-Asr (S'09) received the B.S. degree in electrical engineering from the University of Tabriz, Tabriz, Iran, in 2008. In 2011, he received the M.Sc. degree in control engineering from Tarbiat Modares University, Tehran, Iran, and in 2015, he received the Ph.D. degree in electrical engineering from North Carolina State University, Raleigh, NC, USA.

His research interests include distributed control, distributed optimization, and computational intelligence with application to smart grids.

Chris S. Edrington (S'95–M'04–SM'09) received the B.S. degree in engineering from Arkansas State University, Jonesboro, AR, USA, in 1999, and the M.S. and Ph.D. degrees in electrical engineering from the Missouri Science and Technology, Rolla, MO, USA, in 2001 and 2004, respectively, where he was both a GAANN and IGERT Fellow.

From 2004–2007, he was an Assistant Professor of electrical engineering at the College of Engineering, Arkansas State University. He is currently an Associate Professor of electrical and computer engineering at the FAMU-FSU College of Engineering, Tallahassee, FL, USA, and is the Lead for the energy conversion and integration thrust at the Florida State University-Center for Advanced Power Systems, Tallahassee. Additionally, he is the Florida State University Campus Director for the FREEDM Systems NSF-ERC. His research interests include modeling, simulation, and control of electromechanical drive systems, applied power electronics, distributed control, integration of renewable energy, storage, and pulse power loads.

Mo-Yuen Chow (S'81–M'82–SM'93–F'07) received the B.S. degree in electrical and computer engineering from the University of Wisconsin-Madison, Madison, WI, USA, in 1982, and the M.Eng. and Ph.D. degrees from Cornell University, Ithaca, NY, USA, in 1983 and 1987, respectively.

He joined the Department of Electrical and Computer Engineering, North Carolina State University, Raleigh, NC, USA, as an Assistant Professor in 1987, Associate Professor in 1993, and Professor since 1999. He is a Changjiang Scholar and a Visiting Professor at Zhejiang University, Hangzhou, China. His recent research focuses on distributed control, and fault management on smart grids, batteries, and robotic systems. He has established the Advanced Diagnosis and Control Laboratory, NC State University. He has published one book, several book chapters, and more than two hundred journal and conference articles.

Dr. Chow is a Coeditor-in-Chief of IEEE TRANSACTIONS ON INDUSTRIAL INFORMATICS, Editor-in-Chief of IEEE TRANSACTIONS ON INDUSTRIAL ELECTRONICS 2010–2012. He has received the IEEE Region-3 Joseph M. Biedenbach Outstanding Engineering Educator Award, the IEEE ENCS Outstanding Engineering Educator Award, the IEEE ENCS Service Award, and the IEEE Industrial Electronics Society Anthony J Hornfeck Service Award. He is a Distinguished Lecturer of IEEE IES.